NIH-PA Author Manuscript

Biofunctionalized magnetic-vortex microdiscs for targeted cancer-cell destruction

Dong-Hyun Kim[1], **Elena A. Rozhkova**[2,*], **Ilya V. Ulasov**[3], **Samuel D. Bader**[1,2], **Tijana Rajh**[2], **Maciej S. Lesniak**[3], and **Valentyn Novosad**[1,*]

[1]Materials Sciences Division, Argonne National Laboratory, Argonne, Illinois 60439, USA

[2]Center for Nanoscale Materials, Argonne National Laboratory, Argonne, Illinois 60439, USA

[3]The Brain Tumor Center, The University of Chicago Pritzker School of Medicine, Chicago, Illinois 60637, USA.

Abstract

Nanomagnetic materials offer exciting avenues for probing cell mechanics and activating mechanosensitive ion channels, as well as for advancing cancer therapies. Most experimental works so far have used superparamagnetic materials. This report describes a first approach based on interfacing cells with lithographically defined microdiscs that possess a spin-vortex ground state. When an alternating magnetic field is applied the microdisc vortices shift, creating an oscillation, which transmits a mechanical force to the cell. Because reduced sensitivity of cancer cells toward apoptosis leads to inappropriate cell survival and malignant progression, selective induction of apoptosis is of great importance for the anticancer therapeutic strategies. We show that the spin-vortex-mediated stimulus creates two dramatic effects: compromised integrity of the cellular membrane, and initiation of programmed cell death. A low-frequency field of a few tens of hertz applied for only ten minutes was sufficient to achieve ~90% cancer-cell destruction *in vitro*.

Since the discovery of the compass, magnetic phenomena have become an inseparable feature of everyday life, most noticeably in magnetic recording and advanced information technologies[1]. Nanobiomagnetic applications, including magnetic resonance imaging contrast-enhancement agents, targeted drug delivery, bioseparation and magnetically induced hyperthermia[2–5] are also becoming prominent. Furthermore, magnetic actuation has been explored for 'distant' control and manipulation of cell adhesion, receptor clustering and intercellular signalling[6–8]. Integration of magnetic materials with biological molecules and therapeutics creates hybrid materials with advanced properties[9,10]. Most experimental work so far has used superparamagnetic particles (that is, those with zero magnetic moment at remanence) and their bioconjugates. Because of their superparamagnetic nature and typically small value of the magnetization of saturation, high magnetic fields are required to detect or manipulate these particles. Conversely, if highly magnetic particles are fabricated (that is,

particles with larger single domains), agglomeration may occur owing to magnetic fringe fields. Other challenges related to the traditional approach include difficulty in controlling the growth process, broad size and shape distributions, and variable structural and magnetic properties. Magnetic structures confined to two dimensions, including the arrangement known as a spin vortex, do not suffer from these concerns.

Herein, we report on the interfacing of whole cells with biocompatible lithographically defined ferromagnetic microdiscs (MDs) with a spin-vortex ground state. A magnetic vortex is characterized by an in-plane flux-closure spin distribution with net zero magnetization in the absence of a magnetic field[11−15]. Although the dipole–dipole interaction is known to decrease the vortex state stability for small interdisc separation distances[16], the vanishing magnetization in remanence is significant because this reduces the long-range magnetostatic forces responsible for particle agglomeration. Candidate materials include $3d$ transition metals with high values of the saturation magnetization M_s, because of their ability to induce a high magnetomotive force. When the biofunctionalized MDs selectively bind to cancer cells, this mechanical force is efficiently transduced to the membrane and further on to subcellular components (Fig. 1). We demonstrate that a spatially uniform and time-varying magnetic field as small as tens of oersteds, with a frequency as low as a few tens of hertz and applied for only 10 min, is sufficient to achieve cancer-cell destruction *in vitro*. This antineoplastic activity is the combined result of the compromised integrity of the cellular membrane and magnetic-vortex-mediated initiation of programmed cell death.

The 60-nm-thick, ~1-μm-diameter 20:80% iron–nickel (permalloy) discs, coated with a 5-nm-thick layer of gold on each side, were prepared by magnetron sputtering and optical lithography (ref. [17] and Supplementary Fig. S1) before release from the wafer into aqueous solution, ready for surface modification. Figure 2a shows a representative optical microscope image of the as-fabricated microdiscs dried on a glass slide. The geometry of the sample, combined with intrinsic properties of the permalloy material, results in a magnetic-vortex spin state (Fig. 2b) when the system is in remanence. The magnetic vortex nucleates when the demagnetizing fields within each particle are no longer counterbalanced by the external applied field. The existence of magnetic vortices in our samples was experimentally confirmed by hysteresis-loop measurements (Supplementary Fig. S2) and magnetic-force microscopy imaging of the reference sample (Supplementary Fig. S3). The MDs show zero in-plane magnetic moment in remanence, a linear $M(H)$ dependence in small fields and nucleation and saturation fields of ~250 Oe and ~600 Oe, respectively, in agreement with the model. When a magnetic field is applied, the vortices in each disc shift, developing a magnetization component parallel to the field direction. MDs subjected to a magnetic field **H** will therefore experience a driving torque $\tau_m = \mathbf{m} \times \mathbf{H}$, where **m** is the disc magnetic moment, proportional to both M_s and the magnetic susceptibility. This torque rotates the disc, aligning the plane of the disc parallel to the direction of the magnetic field (Fig. 2d). The dynamics of MDs in aqueous solution were separately investigated before cell-culture experiments. The intensity I of laser light travelling through a vial containing an aqueous MD suspension was monitored as a function of an external magnetic field oriented parallel to the beam. The light transmission increased to I_{max} abruptly whenever the external field was applied; after turning off the applied field, the transmittance fell to I_{min} owing to disc misalignment (Fig. 2e) caused by Brownian motion. Thus, an alternating magnetic field was found to result in modulation of the light intensity $\Delta I = I_{max} − I_{min}$ (Fig. 2c and Supplementary Video). Light-intensity modulation in ferrofluids is known to result from the formation of particle chains in the presence of magnetic fields[18], but this process occurs on a much slower timescale (tens to hundreds of seconds) and therefore is not involved in the experiments reported here. For our sample under ambient conditions, typically a single pulse ~5 ms long of ~10 Oe amplitude achieves complete rotation of suspended discs; the randomness of the disc orientation is recovered ~150 ms after magnetic-field removal. ΔI falls with increasing frequency of the driving field, indicating that the angle of disc rotation decreases

rapidly until at some point the discs become unable to follow the alternating magnetic field (Fig. 2c). Here we are using magnetic-field-driven rotation for controllable mechanical actuation at the cellular level. Gold coating of the discs serves as a biocompatible covering[19] and provides a substrate for easy surface modification of the discs with cancer-targeting ligands.

We have chosen glioblastoma multiforme, an aggressive form of brain cancer, as a model for antineoplastic cell-actuation studies. The specific targeting of MDs to N10 glioma cancer cells[20] was achieved by functionalization of the inorganic material with anti-human-IL13α2R antibody (hereafter referred to as mAb), because IL13α2R is overexpressed on the surface of glioma cells and serves as a marker for targeting by cytotoxic elements, including nanoparticles[21–23]. Thiolate groups that readily react with the gold surface were first randomly introduced into the mAb using N-succinimidyl-S-acetylthioacetate (SATA). After deprotection of the thioacetylated protein, the free thiolate groups of the mAb immediately reacted with the gold surface of the MDs. Owing to the remarkable size difference between an MD surface and a single antibody molecule, the latter was used in 10,000-fold excess. A similar procedure was used to modify the magnetic discs with isotype negative control antibody IgG1, which does not provide specific recognition of glioblastoma multiforme. Enzyme-linked immunosorbent assay indicates that the biorecognition properties of the free mAb were preserved in the final hybrid material MD–anti-IL13α2R (hereafter referred as MD–mAb), reaching ~50% for an isolated IL13α2R and ~45% for N10 glioma cell-line studies (Supplementary Figs S7,S8).

Initial evaluation of the magnetic-field-induced cell death of the MD–mAb relied on assay of cellular lactate dehydrogenase (LDH) released into a medium following the loss of cell-membrane integrity. The N10 glioblastoma multiforme cells were incubated with the MD–mAb on ice for 1 h for binding, washed thoroughly and exposed to a spatially uniform a.c. magnetic field of 90 Oe with a frequency of <60 Hz. In all of experiments described below, ten discs per cell were added, although this is an average number and some of the cells in the culture may have contained no discs at all. After magnetic-field exposure, the cells were cultured under standard conditions for recovery. LDH release was tested after 4 h. No significant effect was observed when MDs functionalized with the isotype-matched negative control IgG1 were used. By contrast, a.c.-magnetic-field-induced MD–mAb showed pronounced cell death as summarized in Fig. 3a. Interestingly, the maximum (~90%) effect was detected at low frequencies (10 and 20 Hz), whereas application of more quickly varying fields (40 and 50 Hz) of the same amplitude resulted in a rapid fall in the LDH release (to ~75% and ~25%, respectively). No significant toxicity was detected at 60 Hz. The falling toxicity with frequency is due to the decrease in disc oscillation amplitude at higher frequencies, when the discs are unresponsive to the rapidly changing field, and thus do not affect the cell-membrane integrity. Using the data on disc rotation obtained in aqueous solution, we estimate an upper limit on the disc oscillation angle to be in the range from 20° down to 5° for driving frequencies from 10 to 50 Hz. The temperature of the cell–MD solution, remotely monitored with an infrared camera, always remained below ~22 °C during our experiments, and varied not more than a few degrees (owing to a small amount of convective heat exchange from the coil) during magnetic-field exposure. This excludes hyperthermia as a possible mechanism of cell damage. The observed LDH leakage might be caused by targeted membrane rupture or 'magnetomechanically induced cell destruction'. Magnetic field exposure times of 10 and 30 min did not affect LDH levels, so 10 min was chosen as the working condition for all further experiments.

Dramatic cell-morphology changes were observed after magnetic-field application. Figure 3 compares representative optical images of the control N10 cells pre-incubated with MD–mAb (Fig. 3b,d) with cells after 90 Oe–20 Hz a.c. magnetic-field exposure following 1 h culture

under standard conditions (Fig. 3c,e). The treated cells are rounded off, with membrane shrinkage and loss of membrane integrity. Furthermore, atomic force microscope images of the fixed cells show that the control $N10$ cells (Fig. 4a) appear as ~500-nm-thick, rough and elongated shapes with well-defined ~1-µm-high nuclei. The treated cells (Fig. 4b) are characterized by an apparent fractioning and redistribution of nucleus material, shape rounding and flattening, surface smoothing and rather abrupt edges. It is apparent that the force produced by slowly oscillating MDs on the cell surface could not alone cause such profound effects. On the basis of a simple magnetic-torque model, we estimate that each disc can deliver a force of the order of tens of piconewtons (see Supplementary Section SIV), whereas the forces needed to rupture a cell membrane are reported to be in the range of hundreds of piconewtons[24–26]. Therefore, it is feasible that the observed effects have not resulted from membrane rupture alone, but instead are due to the triggering of intracellular pathways activating programmed cell death through application of magnetic field to the MD–mAb–cell complex.

Since the observed nucleus fractioning and cell shrinkage are principal morphological characteristics of apoptosis, we assayed one of the hallmarks of late apoptotic cascades, namely genomic DNA fragmentation. To identify nuclear DNA damage, a terminal deoxynucleotidyl transferase dUTP nick end labelling (TUNEL) assay was used[27]. The optical images show that untreated control cells (Fig. 5b,d) with well-organized chromatin structures have a blue fluorescence, whereas treated cells (Fig. 5c,e) are stained with a dark orange–brown dye owing to chromatin fragmentation. Quantified data from TUNEL-positive fluorescent cells are summarized for different a.c.-magnetic-field amplitudes in Fig. 5a. The largest number of TUNEL-positive cells (~60%) was observed for a 90 Oe–20 Hz field. The number of apoptotic cells decreased with further increase in the field strength. We attribute this observation to increasing numbers of necrotic cells at higher field strengths owing to more severe magnetomechanically induced membrane damage. Application of lower fields (30 Oe) still results in a noticeable (~20%) population of cells undergoing apoptosis. The indication of apoptosis was observed both 4 h (Fig. 5) and 24 h (not shown) after magnetic-field exposure. As expected, the number of TUNEL-stained cells was observed to fall remarkably (~50%) after the addition of 20 µM Z-VAD-FMK (carbobenzoxy-valyl-alanyl-aspartyl-[O-methyl]-fluoromethylketone), an inhibitor of caspase proteases, the key players in apoptosis. DNA denaturation at the terminal stage of apoptosis is known to be catalysed by calcium-dependent endonucleases[28], and DNA fragmentation could only barely be directly achieved by the applied mechanical forces. In other words, the observed late apoptotic changes are far removed from the primary stimulus, and therefore are the result of intercellular signal transduction cascades[29].

Calcium signalling is involved in a number of key mechanisms implicated in cell death[29–32]. Stimulus-induced calcium influx through membrane ionic channels, or calcium release from the internal cell sources (for example, the endoplasmic reticulum), can result in the total perturbation of cellular calcium home-ostasis and triggering of apoptosis[29,32]. In the present case, some important apoptosis-related supramolecular membrane structures, including surface 'death' receptors (for example, Fas or TNF-R), or mechanosensitive or other cation channels, may be non-specifically activated by magnetic-vortex-mediated mechanical forces[6–8]. Furthermore, it is well established that membrane disturbances, even if transient and gentle, lead to the induction of stretch-activated channels[33,34], and consequently to increasing levels of intracellular calcium ions[35,36]. Therefore, we investigated whether calcium signalling is involved in the observed magnetic-vortex-driven cell death. For intracellular calcium imaging, $N10$ cells were preloaded with Fluo-4AM, a calcium indicator dye (excitation wavelength $\lambda_{ex} = 488$ nm, emission wavelength $\lambda_{em} = 520$ nm), whereas cell nuclei were stained with Hoechst 33342 ($\lambda_{ex} = 350$ nm). A dual-wavelength laser confocal microscope was used to qualitatively determine changes in calcium intracellular concentration and spatial distribution during magnetic-field application. A magnetic coil was deployed on the microscope sample

stage. All assays were performed in nominally calcium-free Hank's buffer solution. Figure 6a shows an optical micrograph of the imaged area. The initial calcium concentration of cells 1 and 2 seemed to be much lower than that observed in cell 3. This could be true, because the cells were at different stages of their life cycles. To ensure that baseline calcium equilibrium was reached, the dye-loaded cells were imaged for 2 min before magnetic-field application. Next, an alternating magnetic field with a frequency of 10 Hz and amplitude of 90 Oe was applied *in situ* for 10 min to stimulate the biofunctionalized MDs. Cell 3 showed well-pronounced characteristic apoptotic membrane blebbing and shrank significantly during the next few minutes of the experiment. Although its total fluorescence faded by the end of the magnetic-field exposure, owing to cell death or pumping out of calcium and stain, calcium delocalization was clearly observed (for example, compare images Fig. 6b,c). Cells 1 and 2 also showed membrane shrinkage, although to a less significant extent. Significantly, the calcium level in these cells increased, and spectacular dynamic oscillations, spikes and relocalization of calcium were observed (Fig. 6b–d). The most likely explanation is that calcium mobilization arose from intracellular calcium depots, but external calcium pumping cannot be excluded simply because nominally calcium-free buffer was used. Although wide horizons continue to exist, with exciting possibilities for further mechanistic studies, on the basis of our observations we propose that magnetic-vortex-mediated mechanical stimuli are converted and amplified into a chemical ionic signal able to initiate apoptosis and cancer-cell death.

The present study used rather large discs for these proof-of-concept experiments. Because it is well established that the micromagnetic properties of an object fabricated from a given magnetically soft material are determined solely by its geometrical aspect ratio (in the case of MDs, the thickness-to-diameter ratio), the biofunctionalized MD system can be scaled down to smaller lateral dimensions (~100 nm) while preserving its closed-flux spin structure and magnetomechanical properties (ref. [11], and Supplementary Fig. S4).

It is instructive to compare the proposed strategy with the well-explored use of magnetic nanoparticles to achieve tumour regression through hyperthermia effects. The principal remaining problems with magnetic hyperthermia are invasiveness, targeting (restricting the hyperthermia effect to the specific area of interest) and achieving homogenous heat distributions within the target organ[4,5,37−39]. Failure to solve these problems may lead to either insufficient treatment effects or, worse, lethal exposure of neighbouring cells. In contrast to hyperthermia treatment, magnetomechanic stimulus induced by MDs is transmitted directly to the targeted cell with high specificity and high efficiency. Owing to the use of a magnetically soft material with a unique spin arrangement, namely a spin-vortex state, the biologically relevant effect was achieved through application of unprecedentedly weak magnetic fields <100 Oe of a frequency of a few tens of Hz, applied for a duration of only 10 min. This is in stark contrast to the much stronger fields, running at high frequencies of hundreds of kilohertz, required to achieve heating-induced cell toxicity with superparamagnetic particles[37]. In other words, in our experiments, the external power (proportional to $f \times H^2$) supplied to cell cultures was on average at least 100,000 times smaller than that used at present in hyperthermia treatments with magnetic nanoparticles. The low operating field strength may create treatment opportunities with low cost, large working volume, and minimal invasiveness. Because the operating paradigm is not directly mechanical or thermal—instead, the mechanical oscillation of MDs attached to the cancer-cell membrane is transformed into an ionic electrical signal, which triggers the programmed cell-death pathway—the total energy necessary to accomplish cell death is minute. It should be noted, however, that MDs subjected to a.c. field at typical hyperthermia frequencies are likely to demonstrate inductive heating owing to the combined effects of eddy currents and dynamic hysteresis losses. Aside from applications to magnetomechanically induced cancer-cell destruction and hyperthermia, which were discussed, the magnetic microdiscs with a spin-vortex ground state may find further application

in probes of mechanotransduction in cells, distant cell manipulation and separation, controllable force application during regenerative tissue growth and studies of cell elasticity in a diagnostic capacity.

Methods

Biofunctionalization of MDs

27.8 μl of 55 mM SATA solution in dimethyl sulphoxide and 2.8 μl of 60 μM IL13 solution were mixed and incubated at room temperature with continuous gentle shaking in the dark for 30 min. To deprotect thiolate groups the SATA-modified antibody solution was combined with 4 μl of 0.5 M hydroxylamine·HCl and 25 mM ethylenediamine tetra-acetic acid solution in 0.1 M phosphate-buffered saline, pH 7.4, and incubated for 2 h at room temperature. 500 μl of MD suspension (5×10^8 ea ml^{-1}) were degassed by nitrogen gas bubbling for 15 min, and then the deacetylated antibody solution was immediately mixed with the MD suspension with continuous gentle shaking in the dark at room temperature for ~2 h. The final MD–mAb was spin-washed three times with 500 μl 0.1 M phosphate-buffered saline, pH 7.4, to remove unbound protein, and then redispersed in 500 μl of 0.1 M phosphate-buffered saline, pH 7.4, and stored at 4 °C. Fourier transform infrared spectroscopy, wavelength, cm^{-1}: 1650 (amide I) and 1550 (amide II).

Magnetomechanical cell destruction

A magnetic-field station plate was made by inserting a 1/4 inch soft-iron rod into the under-well in a 96-well plate. The station circumference was wound by Cu wire as a coil. The power supply–amplifier (KEPCO, Flushing, NY, USA), function generator (Agilent 33220A, USA) and oscilloscope (Tektronix, Beverton, OR, USA) were connected with the magnetic-field station for generating a.c. magnetic field. For the experiment the 96-well plate with samples was positioned on top of the magnetic-field station plate. Magnetic-field strength was calibrated with a Hall probe. After the treatment, the necrosis and apoptosis of treated cells was assessed with a standard LDH test and TUNEL assay.

Morphological analysis of cell viability by optical and atomic force microscopy

Human glioma cells from the *N*10 cell line were cultivated on poly-ʟ-lysine-coated cover-slips. The human glioma tumour cell line No. 10 cells (*N*10) were grown on the cover-slips in 24-well plates for 24 h to reach 10^4 cells per cover-slip. The cells on the cover-slips were exposed to a.c. magnetic fields as described in the magnetomechanical cell-destruction set-up. The treated cells were fixed in 4% paraformaldehyde and analysed by optical microscopy or recovery cultured in standard conditions for 4 h and then fixed for atomic force microscopy. Cover-slips were thoroughly rinsed with MilliQ water before imaging. Bright- or dark-field images of the cells were taken using ×10, ×20, ×50 and ×100 objective lenses. Atomic force microscope surface images of the cells were acquired in non-contact (tapping) mode.

Laser confocal intracellular calcium imaging

For the calcium assays the *N*10 cells were grown in 35 mm Fluorodish cell-culture dishes (World Precision Instruments, Florida, USA) to reach ~10,000 cells per dish and then incubated with MD–mAb at standard conditions. Cells were loaded with 1 μM Fluo-4-AM containing 0.02% Pluronic F-127 (Molecular Probes) and 1 μg ml^{-1} Hoechst 33342 (Molecular Probes) at 37 °C for 20 and 5 min respectively, washed and then assayed in Hank's buffer. A magnetic coil was placed on top of a sample stage of a dual-wavelength Leica SP5 tandem scanner spectral two-photon confocal microscope. After 2 min of dye-loaded cell initial fluorescence imaging, an alternating magnetic field of 10 Hz (90 Oe) was applied to stimulate MDs on the

cell surface for 10 min. Images were digitized, and fluorescent intensities were analysed using Image J software.

Statistical analysis

All data are expressed as mean ± standard deviation, and were analysed by one-way analysis of variance. Statistical significance was determined, with P values less than 0.05 considered statistically significant.

Supplementary Material

Refer to Web version on PubMed Central for supplementary material.

Acknowledgments

References

1. Chappert C, Fert A, Van Dau FN. The emergence of spin electronics in data storage. Nature Mater 2007;6:813–823. [PubMed: 17972936]

2. Bruns OT, et al. Real-time magnetic resonance imaging and quantification of lipoprotein metabolism *in vivo* using nanocrystals. Nature Nanotech 2009;4:193–201.

3. Ferrari M. Cancer nanotechnology: Opportunities and challenges. Nature Rev. Cancer 2005;5:161–171. [PubMed: 15738981]

4. Pankhurst QA, Connolly J, Jones SK, Dobson J. Applications of magnetic nanoparticles in biomedicine. J. Phys. D 2003;36:R167–R175.

5. Hergt R, Dutz S, Muller R, Zeisberger M. Magnetic particle hyperthermia: Nanoparticle magnetism and materials development for cancer therapy. J. Phys. Condens. Matter 2006;18:S2919–S2923.

6. Dobson J. Remote control of cellular behaviour with magnetic nanoparticles. Nature Nanotech 2008;3:139–148.

7. Mannix RJ, et al. Nanomagnetic actuation of receptor-mediated signal transduction. Nature Nanotech 2007;3:36–40.

8. Wang N, Butler JP, Ingber DE. Mechanotransduction across the cell surface and through the cytoskeleton. Science 1993;260:1124–1127. [PubMed: 7684161]

9. Jun Y-W, Seo J-W, Cheon J. Nanoscaling laws of magnetic nanoparticles and their applicability in biomedical science. Acc. Chem. Res 2008;41:179–186. [PubMed: 18281944]

10. Cheon J, Lee J-H. Synergistically integrated nanoparticles as multimodal probes for nanobiotechnology. Acc. Chem. Res 2008;41:1630–1635. [PubMed: 18698851]

11. Cowburn RP, Koltsov DK, Adeyeye AO, Welland ME. Single-domain circular nanomagnets. Phys. Rev. Lett 1999;83:1042–1045.

12. Shinjo T, Okuno T, Hassdorf R, Shigeto K, Ono T. Magnetic vortex core observation in circular dots of permalloy. Science 2000;289:930–933. [PubMed: 10937991]

13. Wachowiak A, et al. Direct observation of internal spin structure of magnetic vortex cores. Science 2002;298:577–580. [PubMed: 12386329]

14. Buchanan KS, et al. Soliton-pair dynamics in patterned ferromagnetic ellipses. Nature Phys 2005;1:172–176.

15. Ade H, Stoll H. Near-edge X-ray absorption fine-structure microscopy of organic and magnetic materials. Nature Mater 2009;8:281–290. [PubMed: 19308087]

16. Novosad V, et al. Effect of interdot magnetostatic interaction on magnetization reversal in circular dot arrays. Phys. Rev. B 2002;65:060402.

17. Rozhkova EA, et al. Ferromagnetic microdisks as carriers for biomedical applications. J. Appl. Phys 2009;105:07B306.

18. Martin JE, Hill KM, Tigges CP. Magnetic-field-induced optical transmittance in colloidal suspensions. Phys. Rev. E 1999;59:5676–5692.

19. Nel AE, et al. Understanding biophysicochemical interactions at the nano-bio interface. Nature Mater 2009;8:543–557. [PubMed: 19525947]

20. Da K, Shiyama K, Naka R, Hiyama A, Anishi T. GFAP-positive human glioma cell lines: No. 10, no. 11. Hum. Cell 1990;3:251–256.

21. Debinski W, Gibo D, Hulet S, Connor J, Gillespie G. Receptor for interleukin 13 is a marker and therapeutic target for human high-grade gliomas. Cancer Res 1999;5:985–990.

22. Kawakami K, Kawakami M, Snoy PJ, Husain SR, Puri RK. *In vivo* overexpression of IL-13 receptor {alpha}2 chain inhibits tumorigenicity of human breast and pancreatic tumors in immunodeficient mice. J. Exp. Med 2001;194:1743–1754. [PubMed: 11748276]

23. Rozhkova EA, et al. A high-performance nanobio photocatalyst for targeted brain cancer therapy. Nano Lett 2009;9:3337–3342. [PubMed: 19640002]

24. Sen S, Subramanian S, Discher DE. Indentation and adhesive probing of a cell membrane with AFM: Theoretical model and experiments. Biophys. J 2005;89:3203–3213. [PubMed: 16113121]

25. Afrin R, Yamada T, Ikai A. Analysis of force curves obtained on the live cell membrane using chemically modified AFM probes. Ultramicroscopy 2004;100:187–195. [PubMed: 15231309]

26. Muller D, Helenius J, Alsteens D, Dufrêne Y. Force probing surfaces of living cells to molecular resolution. Nature Chem. Biol 2009;5:383–391. [PubMed: 19448607]

27. Mpoke SS, Wolfe J. Differential staining of apoptotic nuclei in living cells: Application to macronuclear elimination in tetrahymena. J. Histochem. Cytochem 1997;45:675–684. [PubMed: 9154154]

28. Yakovlev AG, et al. Role of DNAS1L3 in Ca2+- and Mg2+-dependent cleavage of DNA into oligonucleosomal and high molecular mass fragments. Nucl. Acids Res 1999;27:1999–2005. [PubMed: 10198433]

29. Mattson MP, Chan SL. Calcium orchestrates apoptosis. Nature Cell Biol 2003;5:1041–1043. [PubMed: 14647298]

30. Clapham DE. Calcium signaling. Cell 1995;80:259–268. [PubMed: 7834745]

31. Duchen MR. Mitochondria and calcium: From cell signalling to cell death. J. Phys 2000;529:57–68.

32. Boehning D, et al. Cytochrome c binds to inositol (1,4,5) trisphosphate receptors, amplifying calcium-dependent apoptosis. Nature Cell Biol 2003;5:1051–1061. [PubMed: 14608362]

33. Martinac B. Mechanosensitive ion channels: Molecules of mechanotransduction. J. Cell Sci 2004;117:2449–2460. [PubMed: 15159450]

34. Guharay F, Sachs FJ. Stretch-activated single ion channel currents in tissue-cultured embryonic chick skeletal muscle. Physiol. (London) 1984;352:685–701.

35. Diamond SL, Sachs F, Sigurdson WJ. Mechanically induced mobilization in cultured endothelial cells is dependent on actin and phospholipase. Arterioscler. Thromb. Vasc. Biol 1994;14:2000–2006.

36. Adachi T, Sato K, Tomita Y. Directional dependence of osteoblastic calcium response to mechanical stimuli. Biomech. Model Mechanobiol 2003;2:73–82. [PubMed: 14586810]

37. Hergt R, Dutz S. Magnetic particle hyperthermia—biophysical limitations of a visionary tumour therapy. J. Magn. Magn. Mater 2007;311:187–192.

38. Goya GF, Grazu V, Ibarra MR. Magnetic nanoparticles for cancer therapy. Current Nanosci 2008;4:1–16.

39. Gupta AK, Gupta M. Synthesis and surface engineering of iron oxide nanoparticles for biomedical applications. Biomaterials 2005;26:3995–4021. [PubMed: 15626447]
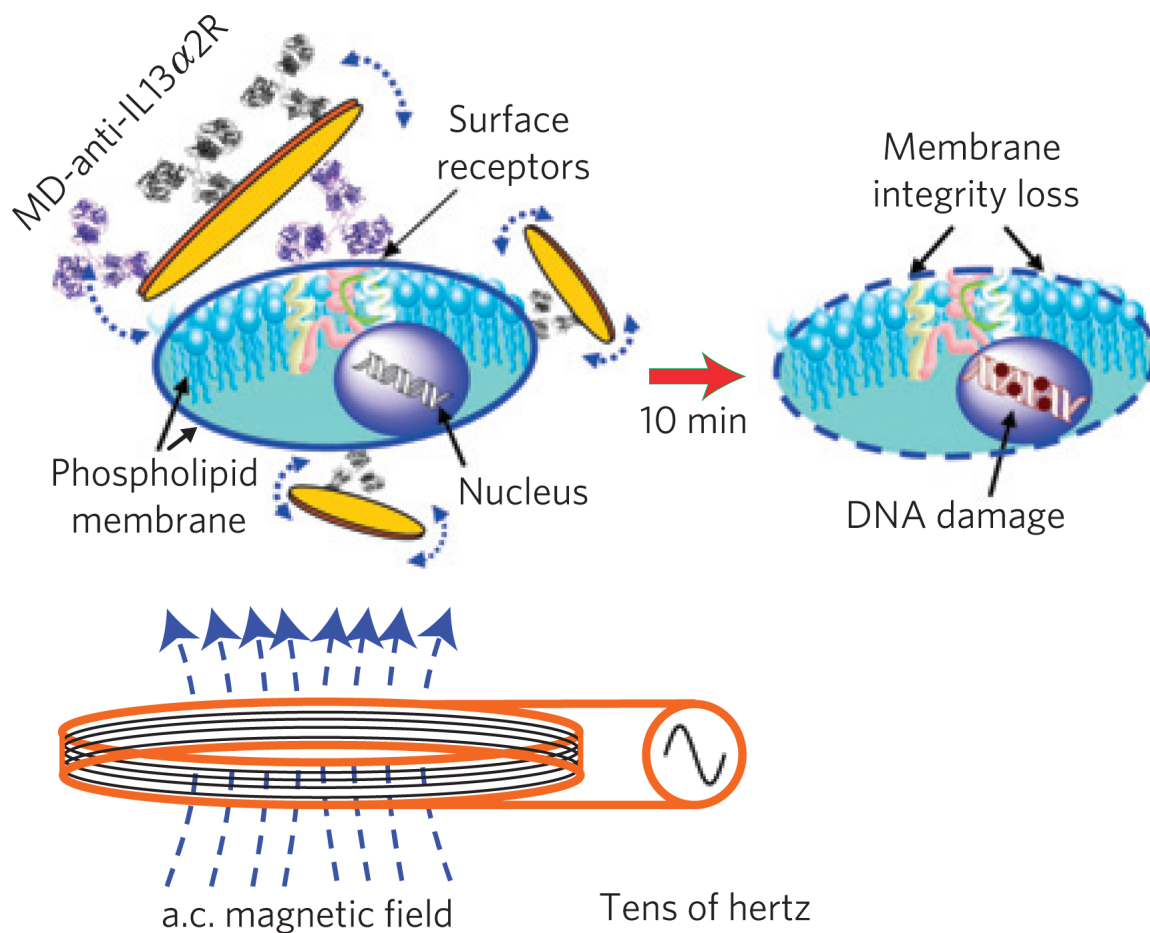
Figure 1. The concept of targeted magnetomechanical cancer-cell destruction using disc-shaped magnetic particles possessing a spin-vortex ground state
The microdiscs are biofunctionalized with anti-human-IL13α2R antibody, specifically targeting human glioblastoma cells. When an alternating magnetic field is applied, the magnetic discs oscillate, compromising membrane integrity and initiating spin-vortex-mediated programmed cell death.
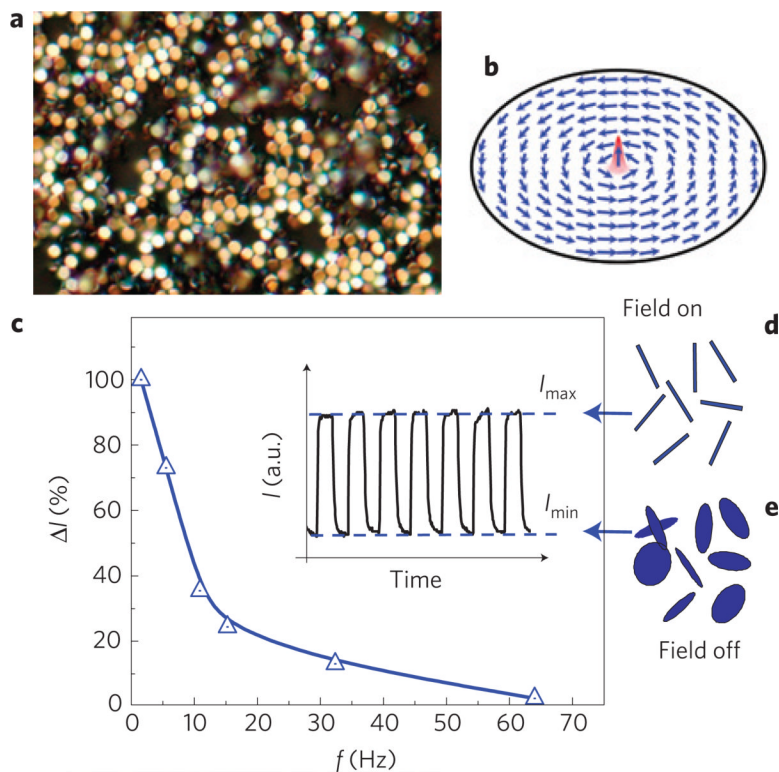
Figure 2. Magnetic-vortex microdiscs can be distantly actuated by the application of small-amplitude and low-frequency a.c. magnetic fields
a, Reflection optical microscope image of the dried suspension of 60-nm-thick, ~1-μm-diameter 20:80 iron–nickel (permalloy) discs coated with a 5-nm-thick layer of gold on each side. The discs were prepared by means of magnetron sputtering and optical lithography. **b**, Micromagnetic model of magnetic-vortex spin distribution. The magnetic vortex consists of a ~10-nm-diameter, perpendicularly magnetized vortex core (Supplementary Fig. S4B), and an in-plane flux-closure spin arrangement with zero net magnetization in the remanent state. **c**, Dependence of the light-intensity modulation $\Delta I = I_{max} - I_{min}$ owing to the field-driven disc alignment (**e–d**) on the applied field frequency f. Inset, A representative time variation of the intensity I of the laser beam travelling through the vial containing the aqueous disc solution subjected to an a.c. magnetic field.
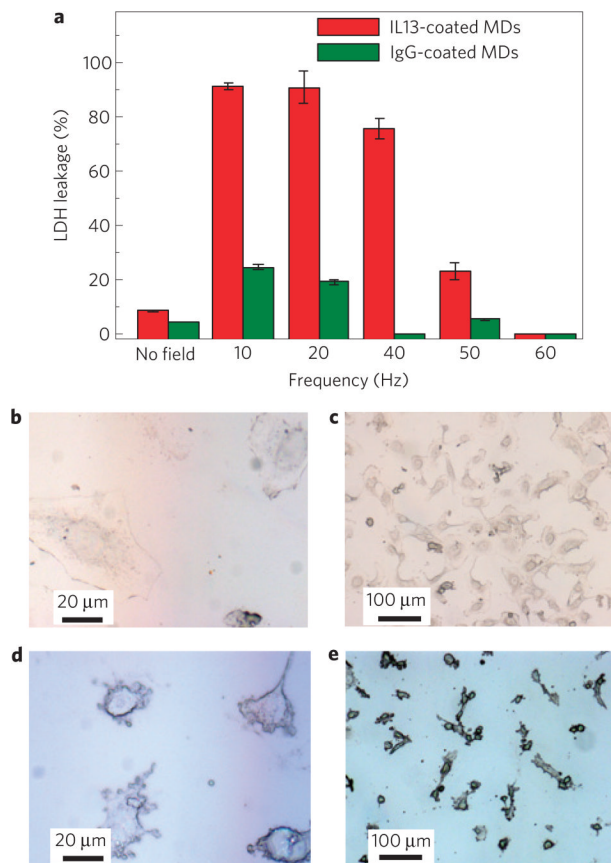
Figure 3. A low-frequency spatially uniform magnetic field applied to the MDs–mAb–cell complex results in compromised integrity of the cellular membrane and cell death

a, Magnetic-field-induced cell death of the MD–mAb towards *N*10 cells and MD-IgG loss of cell-membrane integrity using a cellular LDH test for different field frequencies. No remarkable LDH release was observed when MDs functionalized with the isotype-matched negative control IgG1 were applied. Error bars denote the standard deviation for experiments across six wells. **b–e**, Optical images of control (**b,d**) and treated (**c,e**) *N*10 glioma cells. A 90 Oe–20 Hz magnetic field was applied for 10 min. The treated cells are rounded off with membrane shrinkage and a loss of membrane integrity.
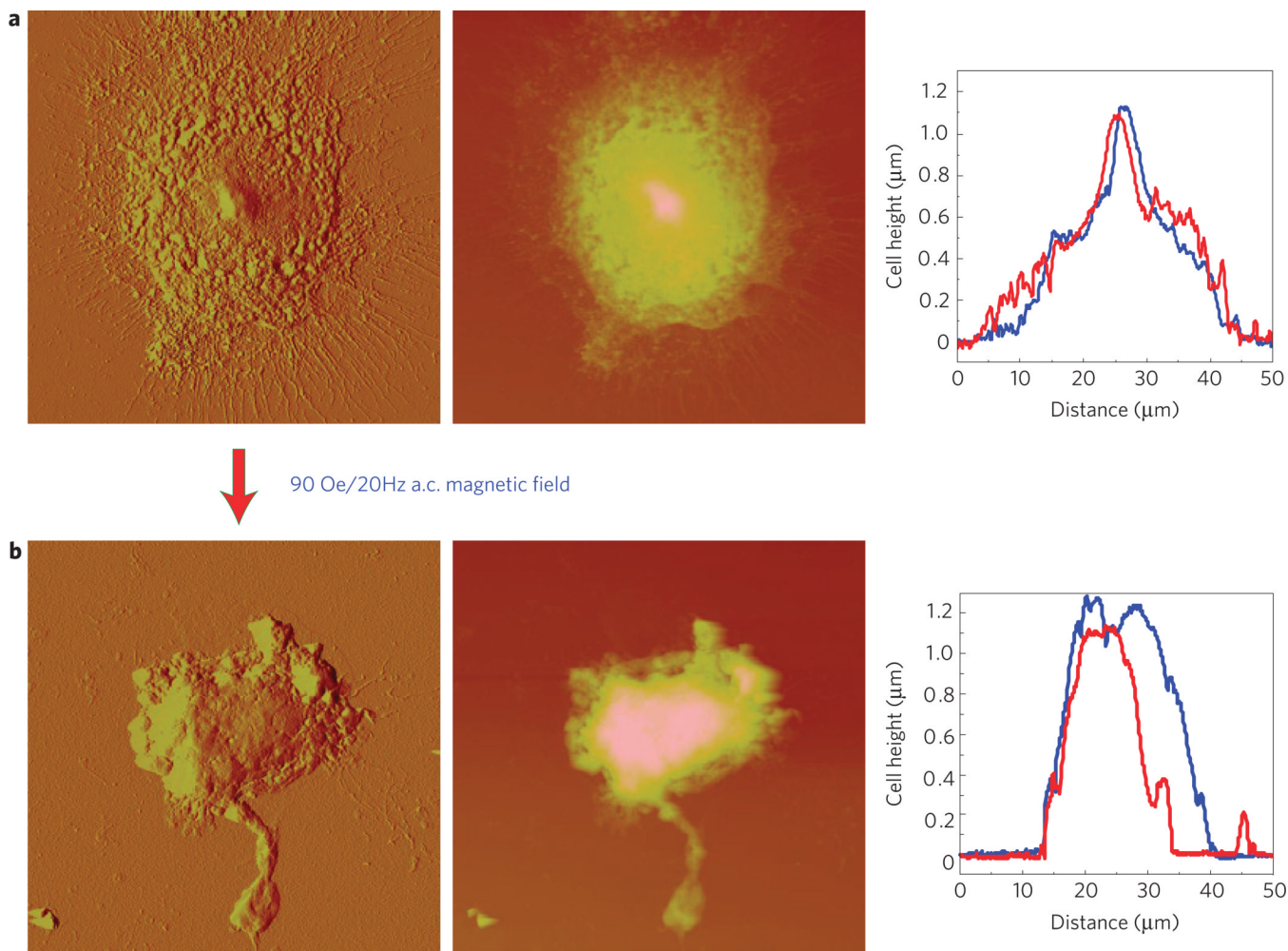
Figure 4. Comparison of representative atomic force microscope amplitude error, height and cross-section scans for the control and treated cells
a, The control *N*10 cells appear as ~500-nm-thick, rough and elongated shapes with well-defined ~1-μm-high nuclei at their centres. **b**, The treated cells are characterized by a smoother surface, thickening, shape rounding, rather abrupt edges and an apparent flattening and fractioning of the genetic material storing organelle—the nucleus. The blue and red curves show the cross-section profiles across the centre of the cell along horizontal and vertical directions, respectively. The scan size is $50{\times}50$ μm^2.
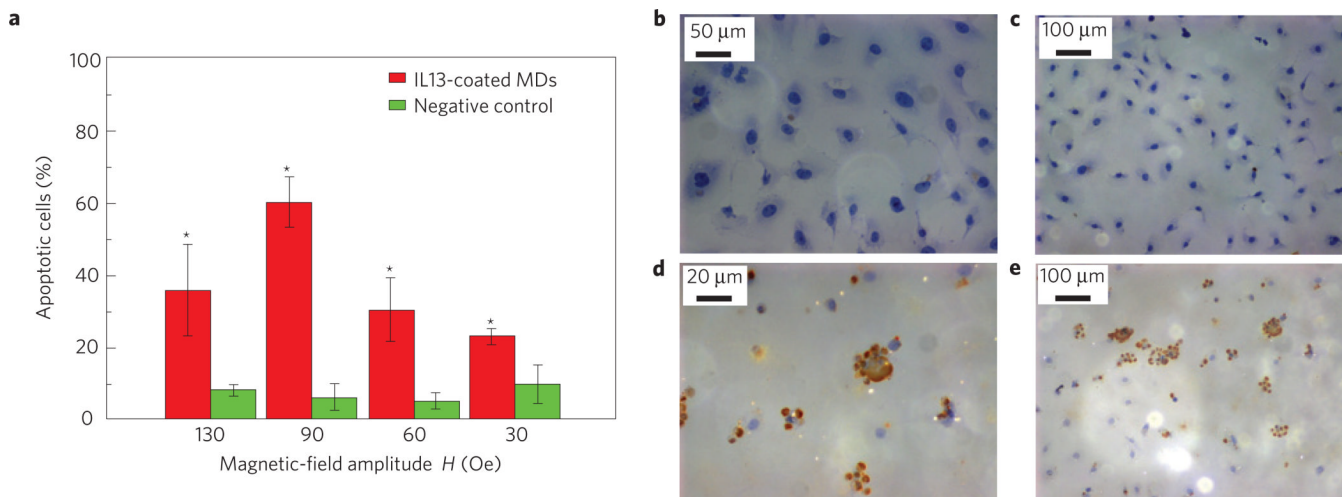
Figure 5. Magnetic-vortex-mediated mechanical stimuli trigger intracellular biochemical pathways activating programmed cell death

a, Apoptosis of the *N*10 cells induced by an a.c. magnetic field. **b–e**, Images of negative control (**b,d**) and MD–mAb-functionalized cells subjected to 20 Hz–90 Oe a.c. fields for 10 min and TUNEL stained 4 h after the magnetic-field exposure (**c,e**). The control cells with well-organized chromatin structures have a blue fluorescence, whereas the treated cells are stained with a dark orange–brown dye owing to chromatin fragmentation—an indication of apoptosis. The proportion of apoptotic populations was calculated by counting a total of 1,000 nuclei in each group using optical microscope images. Error bars denote the standard deviation for experiments across six wells. Asterisks indicate that differences between experimental groups and negative controls were considered significant at $p < 0.05$.
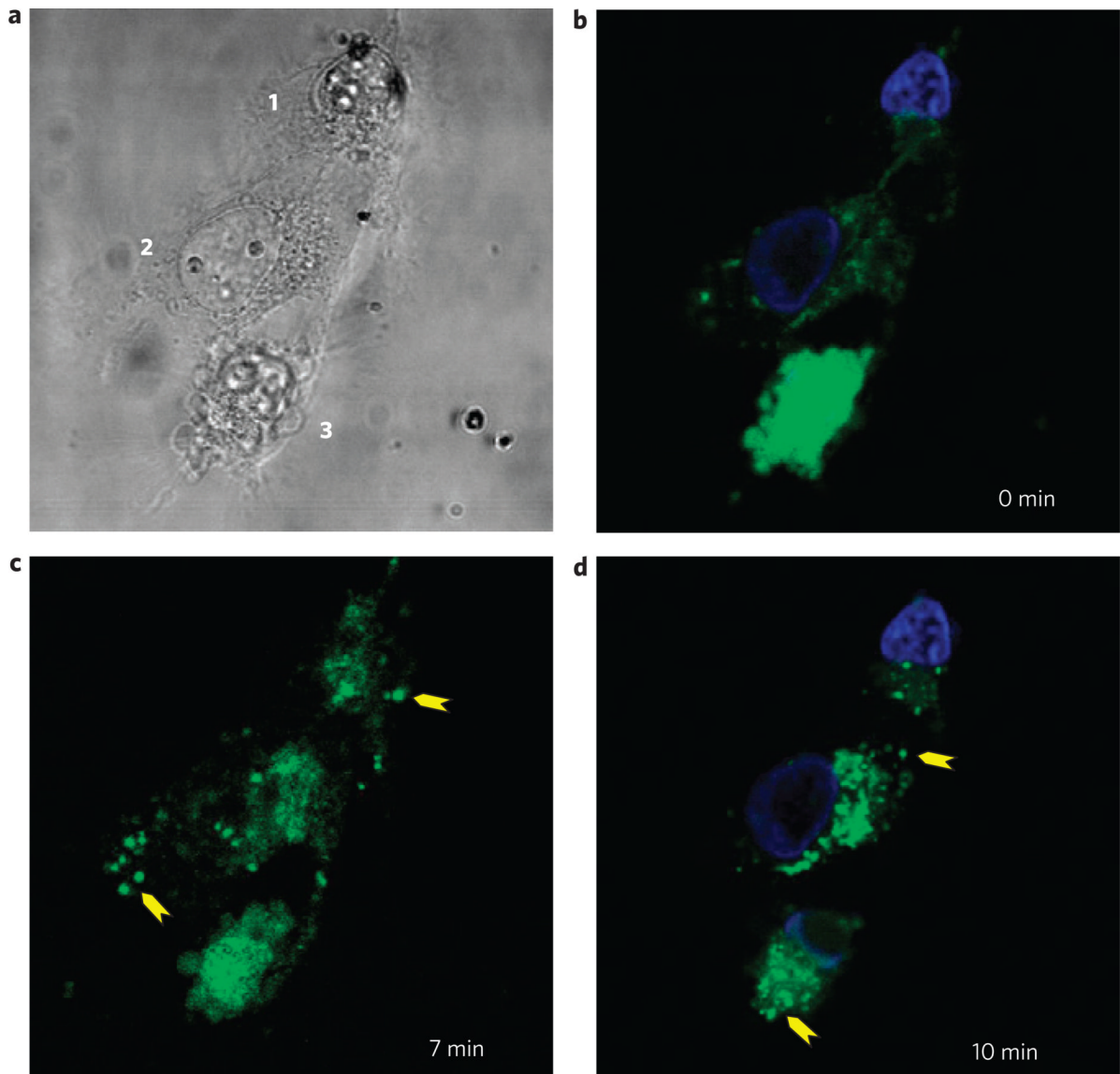
Figure 6. Optical imaging of intracellular calcium

The *N*10 cells were preloaded with calcium indicator Fluo-4-AM dye (λ_{ex} = 488 nm, λ_{em} = 520 nm), green, whereas cell nuclei were stained with Hoechst 33342 (λ_{ex} = 350 nm), blue. **a**, Cell optical images. **b–d**, Fluorescent cell images: snapshots at 0, 7 and 10 min application of alternating magnetic field of 10 Hz–90 Oe. Yellow arrows show representative calcium flashes or spikes.